COBEM 2021 26th International Congress of Mechanical Engineering
ABCM Associação Brasileira de Engenharia e Ciências Mecânicas
November 22-26, 2021, Virtual Congress, Brazil

COB-2021-1961
EXPERIMENTAL EVALUATION OF THERMAL PERFORMANCE AND INTERNAL PRESSURE OF THERMOSYPHONS USING GRAPHENE OXIDE NANOFLUID

Victor Vaurek Dimbarre[1]
Guilherme Antonio Bartmeyer[1]
Pedro Leineker Ochoski Machado[1]
Rozane de Fátima Turchiello[1]
Paulo Henrique Dias dos Santos[2]
Thiago Antonini Alves[1]
Federal University of Technology – Parana (UTFPR), [1]Ponta Grossa/PR, [2]Curitiba/PR, Brazil
victordimbarre@alunos.utfpr.edu.br, pedmac@alunos.utfpr.edu.br, gabartmeyer@hotmail.com, turchiel@utfpr.edu.br, psantos@utfpr.edu.br, antonini@utfpr.edu.br

Abstract. *Thermosyphons are highly efficient passive heat transfer devices capable of transferring thermal energy in small temperature gradients through the latent heat of vaporization, operating in a two-phase cycle. Such devices are composed of an evacuated metallic tube filled with a working fluid. The objective of the present work was to experimentally investigate the influence of working fluid on the thermal performance of thermosyphons and to verify its internal pressure variation. In this study, the working fluids used were distilled water and graphene oxide nanofluid. The devices were manufactured in copper, with an outer diameter of 9.52mm, an inner diameter of 7.94mm, and a length of 515mm. The evaporator had a length of 265mm, while the adiabatic section and condenser had lengths of 70mm and 180mm, respectively. The thermosyphons were filled with 50% of the evaporator volume. The devices were experimentally tested at a slope of 90° from the horizontal under thermal loads ranging from 5 to 25W at the evaporator and cooling of the condenser by air forced convection. The devices also had a pressure transducer attached, which allowed the evaluation of the pressure variation for the different working fluids, and thermal loads. The thermal analysis was based on the temperature distribution along the length, operating temperature, and thermal resistance. The thermosyphon filled with graphene oxide nanofluid presented lower temperature and thermal resistance values, showing itself as the device with the best thermal performance for the experimental conditions it was submitted. The methodology for measuring the internal pressure showed itself satisfactory when comparing the internal pressure of the water-filled device with the analytical vapor pressure, but, regarding both fluids, it was inconclusive which one presented lower internal pressure values due to the experimental uncertainties.*

Keywords: *thermosyphon, internal pressure, thermal performance, nanofluid, graphene oxide*

1. INTRODUCTION

Thermosyphons, also known as gravity-assisted heat pipes, are passive two-phase heat exchange devices that have as the principle of operation the heat transfer from the phase change of a working fluid. Because the heat transfer process occurs from a two-phase flow, it is directly related to the latent heat of vaporization of the working fluid, thus resulting in a high effective thermal conductivity, since the heat transfer coefficients are associated with boiling and condensation are extremely high. These devices are commonly referred to as superconductors, as they possess the ability to transfer high thermal loads with low heat loss along their length (Reay *et al*., 2014).

A thermosyphon consists of a hollow metal tube containing a working fluid. It consists of three different regions along its length: evaporator, adiabatic section, and condenser. It is important to note that thermosyphons are evacuated, operating at low internal pressures (Zohuri, 2016). Figure 1 presents the working principle of a thermosyphon. The evaporator is the lower region of the device, and its function is to absorb heat resulting in the working fluid vaporization process. Due to pressure gradients, the resulting vapor rises at the center of the tube towards the condenser, the coldest region of the device, where the heat absorbed in the evaporator is dissipated to a cooling media, such as water or air flows. As it loses heat, the vapor condenses and returns to the evaporator due to gravity, flowing down the inner walls of the tube, closing the thermodynamic cycle. The adiabatic section is a transition region between the evaporator and condenser, a region where there is no heat exchange with the environment, and sometimes may be absent (Mantelli, 2021).

The process of evaporation and condensation occurs at lower temperatures than the usual ones at atmospheric pressure, due to the very low inside pressure of the device, allowing thermosyphons to operate in a large temperature range, which may also depend on the working fluid used (Kumaresan *et al*., 2014). The correct selection of the working fluid directly

impacts the efficiency of the thermosyphon. Knowing that the working principle of this device is based on the evaporation and condensation of this fluid, some properties deserve special attention at this stage. Among these properties is the latent heat of vaporization, density, viscosity, and conductivity (Faghri, 2014).

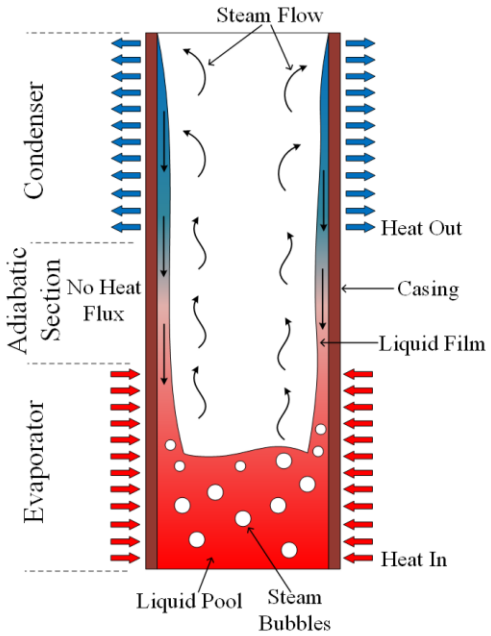

Figure 1. Working principle of a thermosyphon.

The use of nanofluids in heat pipes and thermosyphons can be seen in Khajehpour *et al*. (2020), Chen and Li (2020), Reji *et al*. (2021), and Herrera *et al.* (2021). Nanofluids consist of base fluids with the addition of nanoparticles. Physical properties of the carrier fluid can be improved with the addition of the nanoparticles, such as thermal conductivity, for example. Therefore, nanofluids gain relevance in Thermal Engineering, especially in studies involving the design of heat exchangers. Compared to known conventional fluids, nanofluids presented two main benefits, being them: the increment of heat transfer and smaller surface area required for heat exchangers (Kannadasan *et al.*, 2012; Khairul *et al.*, 2013; Ferreira *et al*., 2018).

Nanofluids can increase the performance of a device such as the thermosyphon and can generate new ranges of application and operation in various equipment (Reay *et al*., 2014; Herrera *et al.*, 2021). The presence of nanoparticles dispersed in a base fluid does not interfere with its latent heat of vaporization or its surface tension, and the operating temperature of the base fluid is similar to that of its nanofluid. Thus, the use of nanofluids can improve the heat transfer of the system when heat exchange by convection and condensation plays an important role (Silva, 2010).

Knowing this, it becomes valid to compare and evaluate the behavior and performance of different working fluids in thermosyphons under different operational conditions. In this study, an experimental investigation of the thermal performance and internal pressure of thermosyphons in different slopes, using distilled water and graphene oxide nanofluid as working fluids is performed.

2. METHODOLOGY

This section describes the characteristics of the thermosyphons and their manufacture process, the synthesis and characterization of the graphene oxide nanofluid, as well as the experimental apparatus and the experimental procedure. The manufacturing methodology of the thermosyphons (cleaning, assembly, tightness test, evacuation process, and filling with the working fluid), experimental tests, and thermal analysis of the thermosyphons were performed taking into account the information contained in Antonini Alves *et al*. (2018).

2.1 Characteristics of the Thermosyphons

The thermosyphons under study were built in copper tubes with a total length of 515mm, an inner diameter of 7.94mm (5/16"), and an outer diameter of 9.52mm (3/8"). The thermosyphons were divided into three parts: evaporator, adiabatic section, and condenser, and their respective dimensions were 265mm, 70mm, 180mm. At the condenser end, an *IFM*™ PN2024 pressure transducer was attached. The working fluids were distilled water and graphene oxide nanofluid, with a filling ratio of 50% of the evaporator volume. Table 1 shows a summary of the characteristics of the thermosyphons under study.

Table 1. Thermosyphon's characteristics.

Parameter	Value
Inner Diameter [mm]	7.94
Outer Diameter [mm]	9.52
Evaporator [mm]	265
Adiabatic Section [mm]	70
Condenser [mm]	180
Working Fluid	Distilled water and graphene oxide nanofluid
Filling Ratio [%]	50

For the cleaning process, first all the parts of the thermosyphon (casing, copper evaporator cover, capillary tube, a steel 3/8" thread hose barb x female swivel ball-end connector, and a steel 1/4" threaded nipple) were cleaned using water and soap for oil and dirt removal. After that, all components, except the casing, were submitted to an ultrasonic bath immersed in acetone, while the interior of the casing was also cleaned using acetone. Finally, the endings of the casing and all the other components were submersed in an 0.1M H_2SO_4 solution for about one minute.

The assembly of the parts was made by the brazing process with tin, using a blowtorch to heat the components. The copper cover was inserted into one end of the casing, while the capillary tube was inserted into a hole present in its center. The 3/8" thread hose barb x female swivel ball-end connector was inserted at the other end of the casing also using the brazing process, and the 1/4" threaded nipple was connected to this connection from its threads, using a thread locking adhesive for sealing (Figure 2).

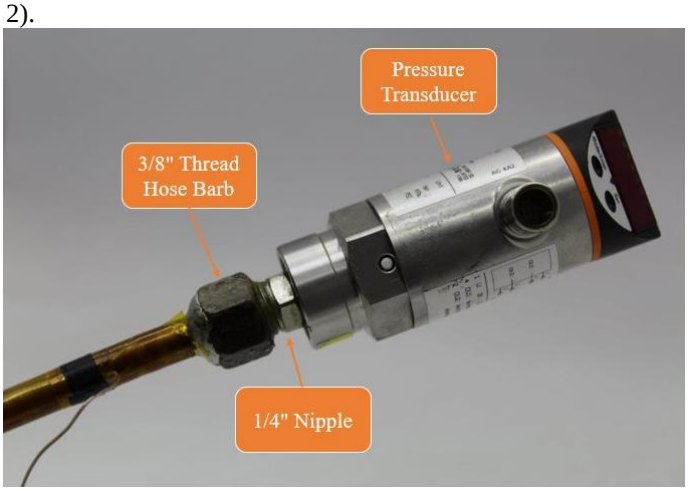

Figure 2. Connection between thermosyphon and pressure transducer.

To ensure that the assembly was done properly and that all connections were completely sealed, the leak test was performed. This test consisted of pressurizing the device while all connections were immersed in water. For this, the capillary tube was connected to a positive displacement pump using a flexible silicone tube, allowing air to be pumped into the device. If bubbles appear in the connections, the assembly process must be redone.

After the leakage test was performed, the device underwent the evacuation process. For this, the thermosyphon was connected to an *EOS Value*™ vacuum pump model i260SV, using *Dow Corning*™ vacuum grease on the connections between the silicone tube, the vacuum pump, and the capillary tube. This process was carried out for approximately 8 (eight) hours, and at the end of this period the silicone tube was sealed with forceps, allowing the thermosyphon to be removed from the vacuum pump.

With the forceps still sealing the tube, it was connected to a graduated burette. Both the free end of the tube and the burette were completely filled with the desired working fluid, and then the connection between them was made so that only working fluid entered the device. After the connection, the valve of the burette was opened and then the pressure exerted by the forceps on the tube was relieved, allowing the passage of fluid.

The thermosyphon was then filled with a filling ratio of 50% of the evaporator volume, sealing the silicone tube again with the forceps, and performing the conformation of the capillary tube with a pressure pliers, not allowing the passage of fluids through its interior. After the conformation process, but with the pliers still exerting pressure on the capillary rube, the free end of the tube was filled with tin, sealing it completely.

2.2 Synthesis and Characterization of the Graphene Oxide Nanofluid

The Hummer's Method (Hummers and Offeman, 1957) was used as the basis for the synthesis of the graphene oxide sample. The main reagents, graphite (CAS 7782-42-5), sulfuric acid (7664-93-9), and potassium permanganate (CAS

7722-64-7) were purchased from *Synth*™. As a result, 1L of a graphene oxide solution with a concentration of 0.00444g/mL was obtained. From this solution, 2.5mL were diluted in 50.0mL of deionized water, which is used in the experiment: 5% graphene oxide nanofluid. The sample has the characteristic absorption bands one at 233nm, related to the π-π* transition of C-C bonds of the aromatic rings, and another at approximately 301nm associated with the n-π* transition of C=O bonds, verified by measurements in a *Femto*™ 800XI UV-Vis Spectrophotometer. Figure 3 presents the data from conventional Scanning Electron Microscopy (*Tescan*™ Vega3) together with the distribution, fitted by a log-normal, which presents a sheet size of 2.9μm along with the high coefficient of variation that is characteristic of this synthesis.

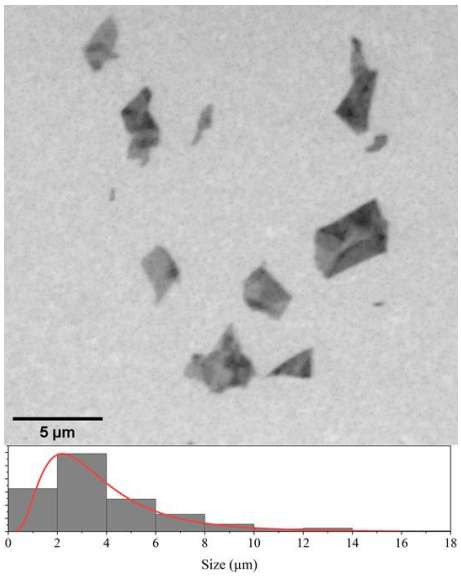

Figure 3. SEM image and particle size distribution of the graphene oxide sheets.

2.3 Experimental Apparatus

The experimental apparatus depicted in Figure 4 was composed of an *Agilent*™ U8002A power supply, a *Keysight*™ DAQ970A data acquisition system with a 20-channel multiplexer, a microcomputer, a fan, and a universal stand with clamps.

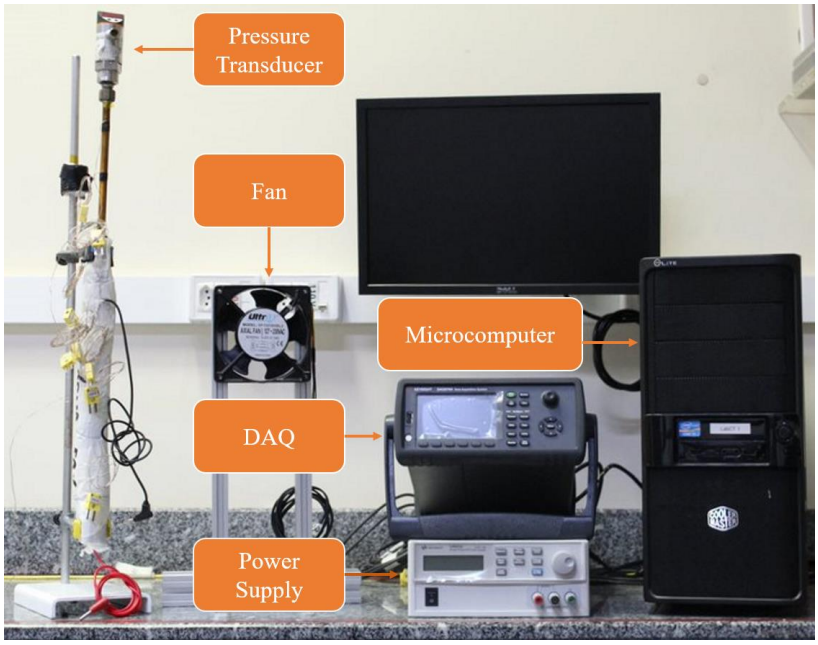

Figure 4. Experimental apparatus.

To evaluate the thermal performance of the thermosyphons, *Omega Engineering*™ K-type thermocouples were used. First, the entire outer wall of the thermosyphon was covered with a *Kapton*™ thermosensitive tape. The thermocouples were then fixed on the outside of the passive device using thermosensitive tape at eight pre-established points (Figure 5), being: four on the evaporator (T_{evap1}, T_{evap2}, T_{evap3}, and T_{evap4}), one in the adiabatic section (T_{adiab}), and three more on the condenser (T_{cond1}, T_{cond2}, and T_{cond3}), besides a thermocouple to obtain the room temperature (T_{amb}).

An *Omega Engineering*™ ribbon resistor (nickel-chromium alloy) with 0.1mm of thickness and 3.5mm of width was wrapped in the hole length of the evaporator, equally spaced and fixed by a thermosensitive adhesive strip. The thermocouples were then adhered to the outer surface of the device, and isolated from the ribbon resistor with a *3M*™ electrical tape. The ends of the resistor were connected to the power supply by test leads with alligator clips. The insulation of the evaporator was made with an *MTI Polyfab*™ aeronautical thermal insulation and a coating of *3M*™ polyethylene, while, in the adiabatic section, *Omega Engineering*™ fiberglass tape was used for the thermal insulation.

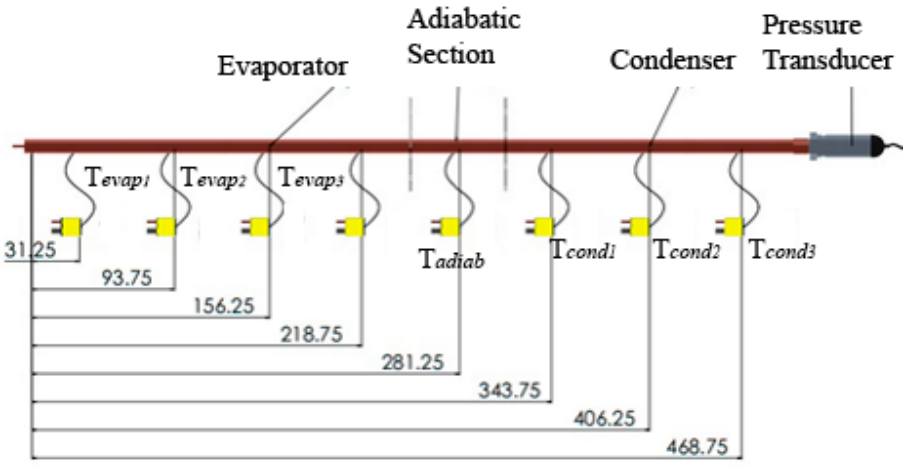

Figure 5. Thermocouple positions [mm].

2.4 Experimental Procedure

With the help of the universal holder, the thermosyphon was fixed by the adiabatic section and placed at 90° with the horizontal. After this, the fan was positioned in the condenser region promoting a forced airflow at a velocity of 1.6m/s measured with an *Itan*™ 720 digital handheld thermal anemometer. To standardize the environmental conditions of all experimental tests, the room temperature was maintained at 16.0±0.5ºC with the help of a *Carrier*™ air conditioning system.

Thermal loads from 5 to 25W, with 5W pitch, were applied to the evaporator region from the Joule Effect resulting from the application of electric power on the resistive tape. Each thermal load was maintained for 20minutes to establish the quasi-permanent regime. Immediately before varying the power dissipated, the pressure showed in the pressure transducer was noted for each power dissipation. Since the pressure displayed on the pressure transducer is the pressure relative to atmospheric pressure, an *Instrutemp*™ *ITWH 1080* weather station (Figure 6) was used for gauging the atmospheric pressure values.

Figure 6. Weather station.

The temperature data acquisition was done by the data acquisition system and saved in the *Keysight*™ *BenchVue* 2020 software with a 10-second interval between each temperature record. To ensure the reliability of the results, for each slope studied, three experimental tests were performed. The thermal analysis was based on the temperature distribution of the thermosyphon versus time for each thermal load, temperature distribution versus length, operational temperature (T_{op}), and thermal resistance (R_{th}).

2.5 Data Reduction

The global thermal resistance of a thermosyphon (R_{th}) can be defined as the ratio of the total temperature drop across the device, the temperature difference between evaporator (T_{evap}) and condenser (T_{cond}), by the rate of total heat transfer, the thermal load applied at the evaporator (q_{in}) – Eq. (1). The higher the thermal resistance, the greater the difficulty in transporting heat from the system (Rohsenow *et al.*, 1998).

$$R_{th} = \frac{T_{evap} - T_{cond}}{q_{in}}. \tag{1}$$

Regarding the experimental results, the combination of parameters that obtains the lowest value of R_{th} is considered the combination with better thermal performance. Furthermore, the operational temperature of a thermosyphon (T_{op}) can be defined as the average working fluid temperature, which is assumed to be equivalent to the adiabatic section temperature (T_{adiab}).

To determine the internal pressure of the device (p_{int}), considering that the values obtained by the pressure transducer are negative, it was obtained from the sum of the atmospheric pressure (p_{atm}) and the relative pressure of the transducer (p_{rel}), as shown in Eq. (2).

$$p_{\text{int}} = p_{atm} + p_{rel}. \tag{2}$$

To validate the internal pressure value obtained from the weather station and the pressure transducer, the vapor pressure (p_{vap}) obtained from an estimate of the vapor temperature (T_{vap}) inside the device was selected. The vapor pressure can be obtained from a system of equivalent thermal resistances of a thermosyphon (Mantelli, 2021), which can be seen in Figure 7. From the thermal resistances observed in this figure, the vapor temperature can be estimated as a function of the flow temperatures outside the evaporator and condenser, $T_{\infty e}$ and $T_{\infty c}$, respectively, in addition to the convection thermal resistances in the evaporator and condenser, R_1 and R_9, respectively, and the conduction thermal resistances in the evaporator and condenser wall, R_2 and R_8, respectively. The determination of the vapor temperature is made from Eq. (3) (Mantelli, 2021).

$$T_v = T_{\infty c} + \left(\frac{R_8 + R_9}{R_1 + R_2 + R_8 + R_9} \right) \left(T_{\infty e} - T_{\infty c} \right), \tag{3}$$

For cases where a constant heat flux is imposed on the outer wall of the evaporator, the value of R_1 is equal to zero, and the evaporator outer wall temperature (T_{eo}) must be taken into account for the calculation of T_v. Thus, according to Machado *et al.* (2020), Eq. (3) can be written as Eq. (4).

$$T_v = T_{\infty c} + \left(\frac{R_8 + R_9}{R_2 + R_8 + R_9} \right) \left(T_{eo} - T_{\infty c} \right), \tag{4}$$

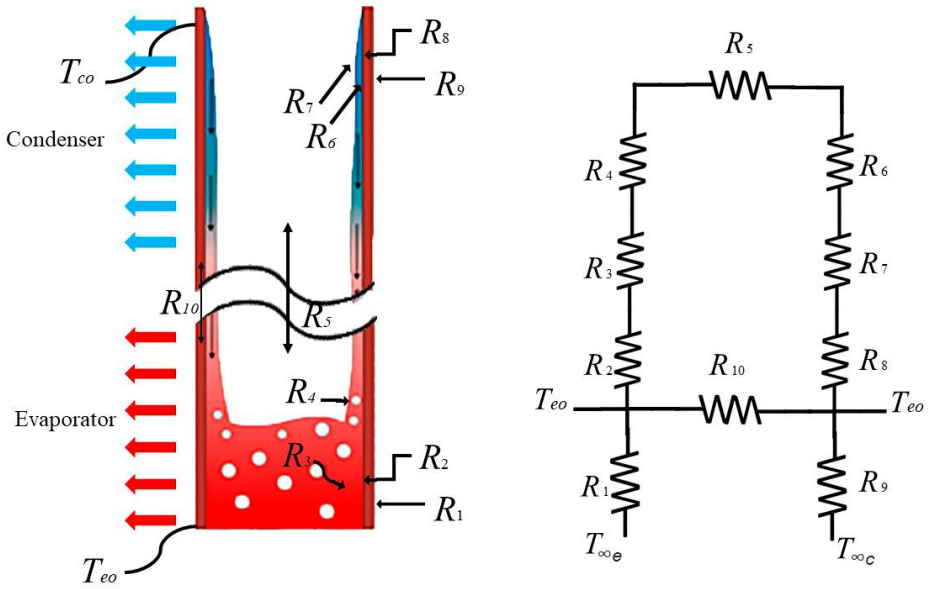

Figure 7. Thermal resistances of a thermosyphon.

The conduction thermal resistances in a hollow cylinder in the evaporator and condenser regions correspond to R_2 and R_8, respectively, and R_9 represents the convection thermal resistance over the condenser, and they can be determined by Eqs. (5,6,7):

$$R_2 = \frac{\ln\left(\frac{d_o}{d_i}\right)}{2\pi L_{evap} k_s}, \tag{5}$$

$$R_8 = \frac{\ln\left(\frac{d_o}{d_i}\right)}{2\pi L_{cond} k_s}, \tag{6}$$

$$R_9 = \frac{1}{h_{e,cond} A_{cond}}, \tag{7}$$

in which d_o and d_i represent the outer and inner diameters of the thermosyphon, respectively; L_{evap} and L_{cond} represent the lengths of the evaporator and condenser, respectively; k_s corresponds to the thermal conductivity of the material that composes the casing (in this case, copper); A_{cond} corresponds to the external area of the condenser; and $h_{e,cond}$ represents the convective coefficient external to the condenser.

The convective coefficient $h_{e,cond}$ was determined using the correlation of Churchill & Bernstein (1977) for the average Nusselt number for external cross flow in cylinders – Eq. (8). This correlation takes into account the Reynolds number of the flow, the thermal conductivity (k), and the Prandtl number (Pr) of the fluid. The Reynolds number of the flow (Re_D), expressed in Eq. (9), was calculated based on the outer diameter of the condenser, specific mass (ρ_{air}), dynamic viscosity (μ_{air}) of the fluid, and the velocity of the flow (u_∞).

$$\overline{Nu}_D = \frac{h_{e,cond} d_o}{k} = 0.3 + \frac{0,62\,\mathrm{Re}_D^{1/2}\,\mathrm{Pr}^{1/3}}{\left[1+(0,4/\mathrm{Pr})^{2/3}\right]^{1/4}}\left[1+\left(\frac{\mathrm{Re}_D}{282000}\right)^{5/8}\right]^{4/5}, \tag{8}$$

$$\mathrm{Re}_D = \frac{\rho_{air} u_\infty d_o}{\mu_{air}}. \tag{9}$$

All the equations were implemented in the *Engineering Equation Solver*™ (EES™) software, where the experimental and geometric parameters related to the experimental tests of the thermosyphon were also entered. From this, the vapor temperature was determined, as well as the vapor pressure, which corresponds to the saturation pressure at $T = T_v$.

2.6 Experimental Uncertainties

In the case of the analysis of uncertainties, results of experimental measurements must carry a measurement uncertainty. This analysis is necessary to estimate the degree of doubt associated with the measurement result. To perform the uncertainty analysis, the uncertainty method described by Holman (2011) was used. With the principle of combining uncertainty of related magnitude, the *Engineering Equation Solver*™ (EES™) software was used to propagate the uncertainties. The uncertainty ΔR of a result $R = f(x_1, x_2, ..., x_n)$ with measures at $x_1,..., x_n$ is expressed by Eq. (10) (Kline and McClintock, 1953).

$$\Delta R = \sqrt{\left(\frac{\partial R}{\partial x_1}\partial x_1\right)^2 + ... + \left(\frac{\partial R}{\partial x_n}\partial x_n\right)^2}. \tag{10}$$

Table 2 presents the precision values considered for each parameter used in the calculations described here. For the millimeter scale, the uncertainty was considered as half of the smallest reading scale, while for the other instruments it was considered what is informed in the literature or technical data sheets provided by manufacturers.

Table 2. Experimental uncertainties.

Parameter	Instrument	Uncertainty	Unit
Temperature	K-type thermocouple	±0.25	°C
Diameter	Pachymeter	±0.5	mm
Length	Millimeter scale	±0.5	mm
Thermal load	Power supply unit	±1%	W
Velocity	Thermal anemometer	±2%	m/s
Pressure	Pressure Transducer	±0.04	bar
Pressure	Weather Station	±3.0	hPa

3. RESULTS AND DISCUSSION

Figures 8(a) and (b) represent the temperature distribution versus time for each thermal load applied for the two working fluids, graphene oxide nanofluid and distilled water, respectively. It can be seen that both devices presented the expected behavior for a thermosyphon. Before the application of the first thermal load, all temperatures were in equilibrium. When the thermal load was applied, the temperatures began to rise, until reaching the steady state, presenting minimal variations in their values. This behavior was repeated for the other thermal loads applied. For all thermal loads the temperatures in the evaporator were higher than in the adiabatic section, which were higher than in the condenser.

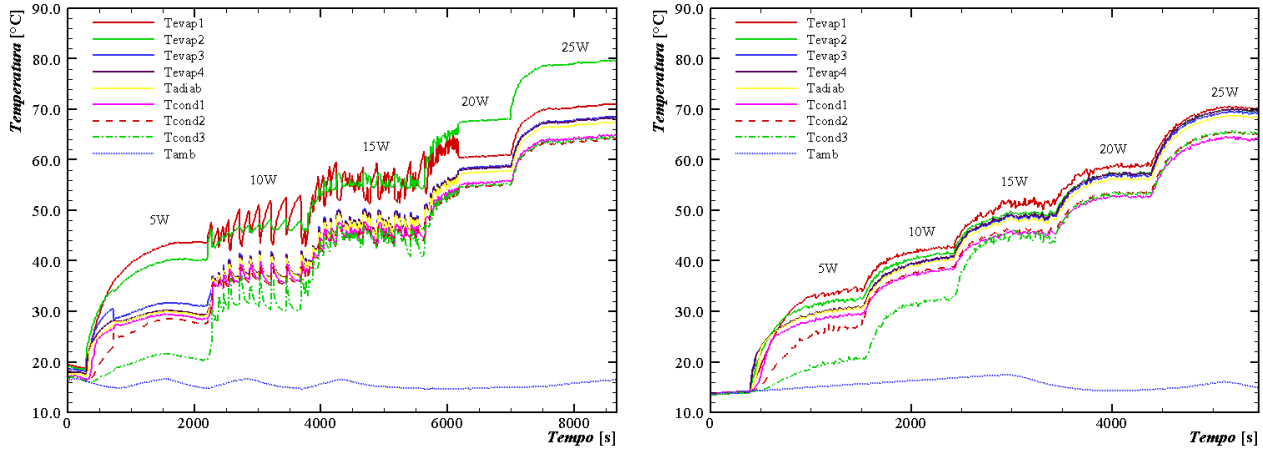

(a) (b)

Figure 8. Temperature distribution versus time: (a) water and (b) graphene oxide nanofluid.

From the comparisons these figures it can be seen that the water-filled thermosyphon took longer to start its operation, the start being evidenced by temperature peaks caused by the geyser boiling effect (Mantelli, 2021). In addition, for all thermal loads the graphene oxide nanofluid filled thermosyphon showed lower temperatures in its regions, which can be considered as an indication that this device showed better thermal performance than the water filled thermosyphon, since lower temperatures indicate that the device has accumulated less energy by transferring the thermal load more efficiently. Table 3 presents the average temperature for each region and each thermosyphon in function of the thermal loads applied.

Table 3. Average temperature of the thermosyphons.

Working Fluid	Thermal Load [W]	Evaporator [°C]	Adiabatic Section [°C]	Condenser [°C]
Distilled water	**5**	36.0	29.6	26.0
	10	43.0	37.9	35.1
	15	51.5	47.2	45.2
	20	61.1	57.2	54.8
	25	71.5	67.0	64.1
Graphene oxide nanofluid	**5**	31.6	30.0	25.1
	10	40.4	39.2	35.6
	15	49.5	47.9	45.4
	20	57.3	56.0	53.0
	25	69.3	68.0	64.5

Figure 9 presents the operational temperature versus thermal load applied for each thermosyphon. As it can be seen, for all thermal loads both working fluids presented very similar values of T_{op}, but, in general, the graphene oxide nanofluid filled device presented higher values of operational temperature.

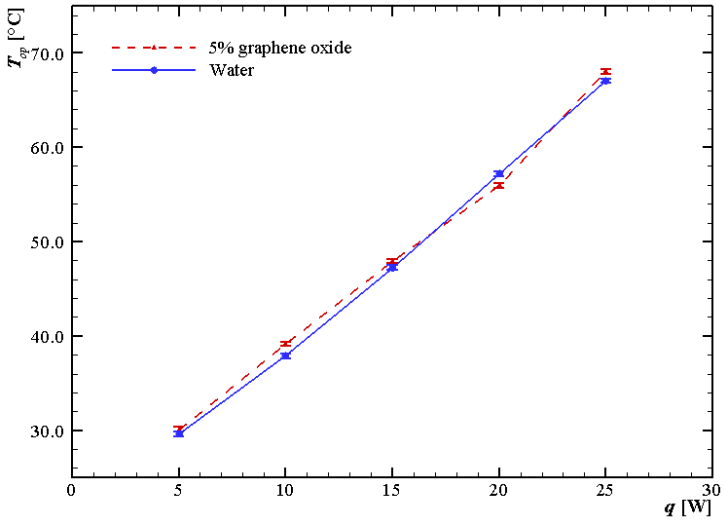

Figure 9. Operational temperature versus thermal load for both working fluids.

Figure 10 presents the thermal resistance results with their respective experimental uncertainty for both fluids as a function of the applied thermal load. Evaluating this figure it can be seen that, for every thermal load, the thermosyphon filled with graphene oxide nanofluid presented lower values of R_{th} than the one filled with distilled water. Equation (1) indicates that, for the same temperature difference between evaporator and condenser, the device with lower thermal resistance can exchange a higher amount of heat, thus, when comparing two different devices, the one with lower R_{th} is considered the one with best thermal performance. In that way, in the conditions tests, the device filled with graphene oxide nanofluid presented the best thermal performance than the one filled with distilled water, corroborating the analysis made about Figure 8. Table 4 presents the thermal resistance values for both working fluids and each thermal load applied.

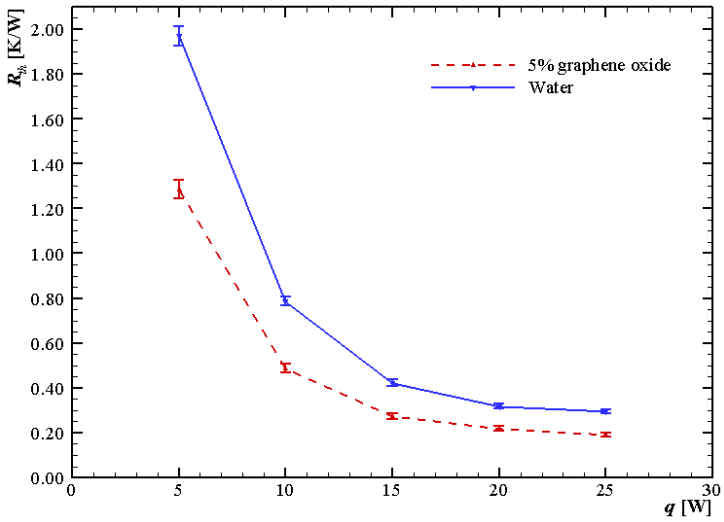

Figure 10. Thermal resistance versus thermal load for both working fluids.

Table 4. Thermal resistance for each working fluids.

Working Fluid	Thermal Load [W]	R_{th} [K/W]	Uncertainty [K/W]
Distilled water	**5**	1.9690	0.0427
	10	0.7871	0.0207
	15	0.4228	0.0134
	20	0.3180	0.0101
	25	0.2943	0.0082
Graphene oxide nanofluid	**5**	1.2860	0.0402
	10	0.4868	0.0197
	15	0.2730	0.0130
	20	0.2185	0.0098
	25	0.1922	0.0079

Figure 11 and Table 5 present the results of internal pressure (p_{int} – Eq. (2)) versus vapor pressure (p_{vap} – obtained from T_{vap} Eq.(4)) for the water-filled device. It can be observed that all p_{int} nominal values remained within a relative difference of less than 25% compared to p_{vap}. This difference is acceptable, since the value of p_{vap} depends on $h_{e,cond}$, and, it is known that the existing correlations in the literature for the calculation of the convective coefficient can present variations of up to 25% (Rohsenow *et al.*, 1998). Thus, it is considered that the methodology used to measure the internal pressure of the device was satisfactory.

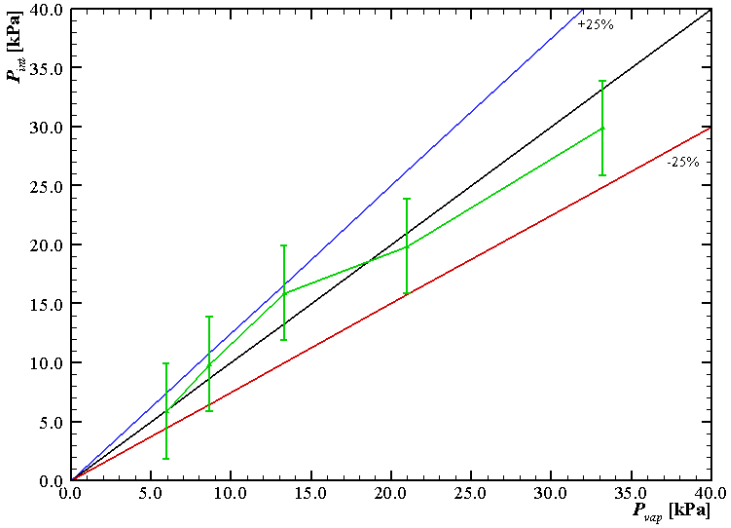

Figure 11. Internal pressure versus vapor pressure for water.

Table 5. Pressure values for the water-filled thermosyphon.

Working Fluid	Thermal Load [W]	p_{atm} [kPa]	p_{rel} [kPa]	p_{int} [kPa]	p_{vap} [kPa]	$(p_{int} - p_{vap})$ [kPa]
Distilled Water	**5**	91.87±0.3	–86±4	5.87±4.01	5.949±0.041	–0.079
	10		–82±4	9.87±4.01	8.646±0.056	1.224
	15		–76±4	15.87±4.01	13.300±0.082	2.570
	20		–72±4	19.87±4.01	20.990±0.120	–1.120
	25		–62±4	29.87±4.01	33.200±0.178	–3.330

Other possible hypotheses for the difference in pressure values is the fact that the analytical p_{vap} calculation considers that the device is filled only with the working fluid, not considering the possibility of the presence of non-condensable gases inside. The presence of non-condensable gases can be due to some facts, such as the fact that the evacuation process does not reach complete vacuum, the presence of dirt inside the device, or the entry of air during the filling process. Another factor that must be taken into account is that the atmospheric pressure is dependent on the ambient temperature. Although the test environment has temperature control, in Figures 8(a) and (b) it is possible to notice some fluctuations in the ambient temperature. In addition, the weather station is located outside the test environment and is not able to capture these variations in atmospheric pressure due to ambient temperature fluctuations. From Table 5 and Figure 11 it can be seen that the difference between p_{int} and p_{vac} values is within the experimental uncertainty of p_{int}, which shows that the methodology used for the internal pressure investigation is satisfactory.

Figure 12 presents the comparison of internal pressure for the thermosyphons filled with graphene oxide nanofluid and distilled water, while Table 6 presents the pressure values obtained for the nanofluid-filled device. From this figure it can be seen that, in general, the nominal values of internal pressure for the device filled with the nanofluid is lower than the one filled with water, which was expected from Table 3, since, from thermodynamics, it is known that the higher the pressure for a fluid, the higher its temperature. Nevertheless, due to the measurement uncertainties, it is inconclusive which fluid has the lower pressure, since, because the uncertainty bars cross, statistically the two devices showed the same pressure for all applied thermal loads.

Table 6. Pressure values for the thermosyphon filled with graphene oxide nanofluid.

Working Fluid	Thermal Load [W]	p_{atm} [kPa]	p_{rel} [kPa]	p_{int} [kPa]
Distilled Water	**5**	91.87±0.3	–88±4	3.87±4.01
	10		–84±4	7.87±4.01
	15		–80±4	11.87±4.01
	20		–74±4	17.87±4.01
	25		–62±4	29.87±4.01

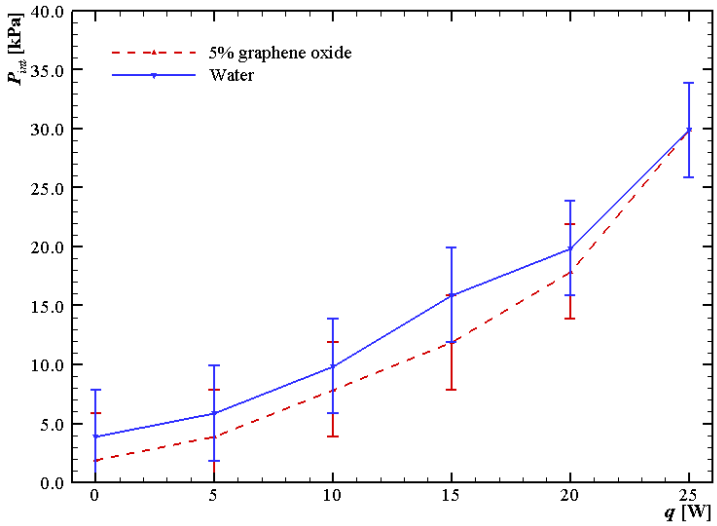

Figure 12. Internal pressure versus thermal loads for both fluids.

4. CONCLUSION

This study described the construction of thermosyphons made in a copper tube and filled with distilled water and graphene oxide nanofluid, containing a pressure transducer on its end for measuring the internal pressure of the passive heat transfer devices. The thermosyphon was tested at a 90° slope with the horizontal, with heat dissipation over the evaporator resulting from power dissipation over a resistive ribbon, and cooling of the condenser through forced convection with atmospheric air. The performance of the thermosyphon with each working fluid was verified from thermal analysis, taking into account the temperature distribution in the device as a function of time, operating temperature, thermal resistance, and internal pressure as a function of the thermal load applied to the evaporator region. From the thermal analysis, it was experimentally verified that, for the operational conditions applied and the characteristics of the thermosyphons, the device filled with the 5% graphene oxide nanofluid presented lower temperatures at its regions, and also lower values of thermal resistance, being the device with a better thermal performance. Regarding internal pressure results, the experimental internal pressure of the water-filled device was compared with the analytical vapor pressure obtained through the association of thermal resistances of the thermosyphon. It was found that the methodology used for measuring the internal pressure was satisfactory, since the difference between p_{int} and p_{vap} was within the experimental uncertainty. Comparing both working fluids, it was inconclusive which fluid presented lower internal pressure also due to the experimental uncertainty.

5. REFERENCES

Antonini Alves, T., Krambeck, L., and Santos, P.H.D., 2018. “Heat pipe and thermosyphon for thermal management of thermoelectric cooling”. In: Aranguren, P. (Org.). *Bringing thermoelectricity into reality*. InTech, London.

Chen, M., and Li, J., 2020. “Nanofluid-based pulsating heat pipe for thermal management of lithium-ion batteries for electric vehicles”. *Journal of Energy Storage*, Vol. 32, December, 101715.

Churchill, S.W., and Bernstein, M.A., 1977. “A correlating equation for forced convection from gases and liquids to a circular cylinder in crossflow”. *Journal of Heat Transfer*, Vol. 99, No. 2, pp. 300–306.

Faghri, A., 2014. “Heat pipes: review, opportunities and challenges”. *Frontiers in Heat Pipes*, Vol. 5, No.1, pp. 1–48.

Ferreira, T.P.A., Fogaça, M.B., Lenart, V.M., Behainne, J.J.R., Gomez, S.L., and Gomez, R.F.T., 2017. “Design and construction of a heat exchanger: use of nanofluids (gold nanoparticles in base fluid)”. In *Proceedings of the 24th International Congress of Mechanical Engineering – COBEM* 2017. Curitiba, Brazil.

Herrera, B., Gallego, A., and Cacua, K., 2021. “Experimental evaluation of a thermosyphon-based heat exchanger working with a graphene oxide (GO) nanofluid in a cogeneration system”. *Thermal Science and Engineering Progress*, Vol. 24, August, 100949.

Holman, J.P., 2011. *Experimental methods for engineers*, McGrall-Hill, New York.

Hummers, W.S., and Offeman, R.E., 1957. “Preparation of graphitic oxide”. *Journal of the American Chemical Society*, Vol. 208, No. 1937, pp. 1937.

Kannadasan, N., Ramanathan, K., and Suresh, S., 2012. “Comparison of heat transfer and pressure drop in horizontal and vertically helically coiled heat exchanger with CuO/water based nano fluids”. *Experimental Thermal and Fluid Science*, Vol. 42, October, pp. 64–70.

Khairul, M.A., Saidur, R., Rahman, M.M., Alim, M.A., Hossain, A., and Abdin, Z., 2013. "Heat transfer and thermodynamic analyses of a helically coiled heat exchanger using diferente types of nanofluids". *International Journal of Heat and Mass Transfer*, Vol. 67, December, pp. 398–403.

Khajehpour, E., Noghrehabadi, A.R., Nasab, A.E., Nabavi, S.M.H., 2020. "Experimental investigation of the effect of nanofluids on the thermal resistance of a thermosiphon L-shape heat pipe at different angles". *International Communications in Heat and Mass Transfer*, Vol. 113, April, 104549.

Kline, S.J., and McClintock, F.A., 1953. "Analysis of uncertainty in single-sample experiments". *Mechanical Engineering*, Vol. 75, pp. 3–8.

Kumaresan, G., Venkatachalapathy, S., Asirvatham, L.G., and Wongwises, S., 2014. "Comparative study on heat transfer characteristics of sintered and mesh wick heat pipes using CuO nanofluids". *International Communications in Heat and Mass Transfer*, Vol. 57, October, pp. 208–215.

Machado, P.L.O., Souza, R.O., Szmoski, R.M., Machado, V.O.O., and Antonini Alves, T., 2020. "Comparison of the experimental performance of a thermosyphon with its thermal design". In *Proceedings of the 18th Brazilian Congress of Thermal Sciences and Engineering* – ENCIT 2020. Rio de Janeiro, Brazil.

Mantelli, M.B.H., 2021. *Thermosyphons and heat pipes: theory and applications*. Springer Nature Switzerland, Cham.

Reay, D.A., Kew, P.A., and McGlen, R.J., 2014. *Heat pipes: theory, design and applications*. Elsevier, Waltham.

Reji, A.K., Kumaresan, G., Sarathi, A., Saiganesh, A.G.P., Kumar, R.S., and Shelton, M.M., 2021. "Performance analysis of thermosyphon heat pipe using aluminum oxide nanofluid under various angles of inclination". *Materials Today*: *Proceedings*, Vol. 45, Part 2, pp. 1211–1216.

Rohsenow, W.M., Hartnett, J.P., and Cho, Y.I., 1998. *Handbook of heat transfer*. McGraw-Hill, New York.

Silva, A.C.M., 2010. *Heat transfer in nanofluids – potentialities and challenges* (in Portuguese). Master's Dissertation, Graduate Program in Chemical Engineering, University of Aveiro, Aveiro, Portugal.

Zohuri, B., 2016. *Heat pipe design and technology - modern applications for practical thermal management.* Springer Nature Switzerland, Cham.

6. RESPONSIBILITY NOTICE

The authors are the only responsible for the printed material included in this paper.